Indonesian Journal of Electrical Engineering and Informatics (IJEEI)
Vol. 12, No. 2, June 2024, pp. 333~343
ISSN: 2089-3272, DOI: 10.52549/ijeei.v12i2.5520

Flexible Potentiostat Readout Circuit for Electrochemical Sensors

Nur Hanisah Azmi[1], Anis Nurashikin Nordin[2], Muhammad Irsyad Suhaimi[3], Lim Lai Ming[4], Rosminazuin Ab Rahim[5], Zambri Samsudin[6], Aliza 'Aini Binti Md Ralib @ Md Raghib[7]
[1,2,5,7] VLSI-MEMS Research Unit, Department of Electrical and Computer Engineering, Engineering Faculty, International Islamic University, Malaysia
[3]Jabil Customer Solutions Center, United States of America
[4,6]Manufacturing Technology & Innovation (MTI), Jabil Circuit Sdn Bhd, Malaysia

Article Info

Article history:

Received Mar 31, 2024
Revised Jun 1, 2024
Accepted Jun 6, 2024

Keywords:

Flexible printed circuit board
FPCBs
Potentiostat
Biosensing applications
Cyclic voltammetry

ABSTRACT

Personalised health wearables reach their full potential when sensors are integrated with its interfacing system. Recent approaches have primarily focused on the development of readout circuits limited to the electrochemical chip and basic signal conditioning components. However, integrating a readout circuit with a microcontroller offers significant advantages such as enhanced data processing capabilities. Other than incorporating a microcontroller within the readout circuit, we also designed the entire potentiostat system on a flexible polyimide substrate, making it suitable for wearable applications. In this work, we describe the design, fabrication and testing of a flexible potentiostat readout circuit for electrochemical sensors. The core of the interface circuit is two chips, a microcontroller ATSAMD21G18A-MUT (Microchip Technology) and a programmable analog front-end integrated circuit from Texas Instruments. These chips along with a voltage regulator, resistors and capacitors were integrated onto a single, flexible, printed circuit board. To verify the functionality of the flexible readout circuit, it was connected to an electrochemical sensor and Cyclic Voltammetry (CV) was performed. The separation between peaks (ΔE_p), were measured using the flexible board and compared with a commercial potentiostat (Emstat Pico). EmStat Pico has ΔE_p = 0.133V, while our potentiostat produced ΔE_p of 0.132V, indicating minimal variations with the same PCB layout, despite using different substrates. The standard rate constant (K_s) of electron transfer can also be obtained from CV and was measured to be 0.0037 for the rigid PCB and 0.0035 for the flexible PCB.

Corresponding Author:

Anis Nurashikin Nordin,
Department of Electrical and Computer Engineering,
International Islamic University Malaysia,
Jalan Gombak, 53100 Kuala Lumpur.
Email: anisnn@iium.edu.my

1. INTRODUCTION

A readout circuit is an important component in various sensing systems, especially for signal conditioning or data processing. Traditionally, the readout circuit was limited to the electrochemical chip and basic signal conditioning components [1], [2]. However, integrating a microcontroller into the readout circuit offers significant advantages, such as enhanced data processing capabilities, improved signal-to-noise ratios and seamless communication with external devices. In addition to having an advanced readout circuit integrated with a microcontroller, its utility is further enhanced when implemented on a flexible substrate, making it suitable for wearable applications.

Flexible Printed Circuit Boards (FPCBs) is a rapidly growing field that holds immense potential for various applications such as healthcare, consumer electronics, automotives and wearable technology [3], [4]. FPCBs are advantageous as their circuit boards have freeform and can be either folded, twisted or moulded into any desired shape. The most common type of PCB is a rigid one made of flame-retardant material (FR-4), but recent studies have focused primarily on the reliability of FPCBs made of polyimide film (PI) [5]. FPCBs offer unique benefits compared to their rigid counterparts as they can follow the form of any irregularly shaped substrate such as an automobile or the human body [3]. Compared to rigid PCBs [6], FPCBs are lightweight and portable and are made to withstand numerous bend loadings [4]. FPCBs are commonly formed by a conductive layer of traces made up of copper coupled with a polyimide dielectric layer [5], [7]. Amongst the many applications of FPCBs, of recent interest is its usage with electrochemical biosensing systems [7].

Recently, researchers have been actively working towards having fully integrated electrochemical sensing systems that can merge the fields of modern healthcare, consumer bioelectronics and human-machine interfaces [8], [9], [10], [11]. Most of existing research focuses on implementation of flexible sensors such as flexible Organic Electrochemical Transistors (OECTs) [6], strain sensors [12], glucose sensors [13] and pressure sensors [14]. Electrochemical biosensing systems often require interfacing circuitry to process the data. Combining the sensing and electronic modules on the same platform can drastically reduce its form factor making it ideal for portability and wearability [15].

Potentiostats are an essential analytical tool for electrochemical measurements and are commonly used to control most electroanalytical experiments. The presence of electrochemically active compounds, viruses and microbes in sample solution can be detected using potentiostat. A typical electrochemical setup uses a two/three-electrode sensor. The potentiometric signals are applied by the potentiostat to initiate a reaction between an analyte and a surface, and the measured output current correlates with the analyte concentration [16]. However, existing potentiostats are often bulky and rigid [17]. Recognizing this limitation, this research focuses on developing portable potentiostats using FPCBs. This was done by reducing the complexity of traditional potentiostats and the number of its components.

Previous researchers have designed relatively low-cost potentiostats using off-the-shelf microcontrollers and potentiostat integrated circuits (ICs) [6], [18], [19], [20]. SIMstat and MiniStat are some examples of affordable and portable potentiostats, which were designed to make electrochemical analysis more accessible [18], [19]. The complexity of the readout circuits depends on the different types of electrochemical measurements that the device can perform. For example, SIMstat conducts real-time Cyclic Voltammetry (CV), while MiniStat can perform CV, ChronoAmperometry (CA), and Square Wave Voltammetry (SWV) with relatively low power consumption. Another notable potentiostat is ABE-Stat, which can perform Electrochemical Impedance Spectroscopy (EIS) measurements across a wide frequency range [20][21]. SenSARS is another potentiostat which can also perform electrochemical impedance spectra measurement [22]. Finally, there is KickStat, a miniature potentiostat which can perform a variety of electrochemical measurements such as CV, SWV, CA and Normal Pulse Voltammetry (NPV) [6], [23]. All the above circuits were implemented on rigid PCBs.

With the advent and popularity of wearables and automotive electronics, there is a need for PCBs to be more freeform and able to conform to the substrate that it is placed upon. Rigid PCBs are less versatile, thicker, heavier and cannot adapt to curvilinear or irregular shapes. Their bulkiness can be a significant limitation, especially in applications where size and weight are critical factors. In contrast, FPCBs offer a lightweight and adaptable solution, making them more suitable for applications requiring flexibility such as wearable electronics. Table 1 provides the comparison between PCBs and FPCBs, highlighting the advantages of FPCBs. FPCBs can withstand various environmental conditions, including temperature variations and mechanical stress, while providing good electrical performance compared to traditional rigid PCBs [24].

An example of a flexible potentiostat readout circuit patch had been demonstrated in [1], and used for pH measurements. This circuit is capable of performing simple pulse voltammetry. In contrast, our work describes the implementation of a potentiostat circuit which can perform cyclic voltammetry (CV). CV is a fundamental electrochemical technique that is often performed to study the kinetics of electrochemical reactions through reduction and oxidation processes. It provides valuable insights into the redox behaviour and electrochemical characteristics of a system which involves the exchange of electrons between species in solution and the electrode surface [25]. The shape and symmetry of the CV curves indicate whether the reactions are reversible, quasi-reversible, or irreversible, providing information about reaction mechanisms and kinetics [26]. The peak potentials and peak currents in CV curves provide information about the kinetics of electrode reactions. The separation between anodic and cathodic peak potentials (ΔE_p) indicate the rate of electron transfer at the electrode surface. Analysis of the CV curves can also be used to study the standard electron transfer rates, or standard rate constants, K_s.

Table 1. Comparison between Printed (PCB) and Flexible Printed Circuit Board (FPCB)

Substrate	Advantages	Limitations
FPCB	Fewer maintenance interventions. Elimination of conventional wire connections. Higher and longer-term reliability. Size, weight, and manufacturing time reduction.	The troubleshooting process is complicated. Less adjustment can be made as the flexible substrate is more delicate. More expensive.
PCB	Built of solid materials that add rigidity and longevity to the board. Cost-effective. Easier to debug and repair.	Cannot bend, twist or fold. Long production time. Increased circuit size, weight, and complexity.

This paper describes the design, fabrication, and integration of a potentiostat on flexible PCB. The manuscript is organised into five sections. Section 1 provides an overview of flexible PCBs in various applications, followed by review of existing potentiostat technologies. In Section 2, the flexible potentiostat design specifications are presented. Section 3 focuses on the experimental work using the designed flexible potentiostat, which has been fabricated on both rigid PCB and FPCBs. In Section 4, the results and discussions are presented which includes a comparison between the rigid PCB and FPCBs designs. It also discusses the final results obtained from the cyclic voltammetry measurements using the fabricated potentiostat and EmStat Pico boards.

2. DESIGN OF FLEXIBLE READOUT CIRCUIT FOR ELECTROCHEMICAL SENSOR

The design work for the readout circuit for the electrochemical sensor starts with its schematic design, PCB layout, board fabrication, firmware development and finally testing and valdation as shown in Fig. 1(a). The block diagram of the potentiostat system is divided into two parts: the potentiostat itself and the electrochemical biosensor named IEQCM sensor, as illustrated in Fig. 1(b). The core of the potentiostat comprises the electrochemical sensor integrated circuit (IC) (LMP91000SD/NOPB - Texas Instruments), overseen by a low-power yet high-performance microcontroller (ATSAMD21G18A-MUT - Microchip Technology).

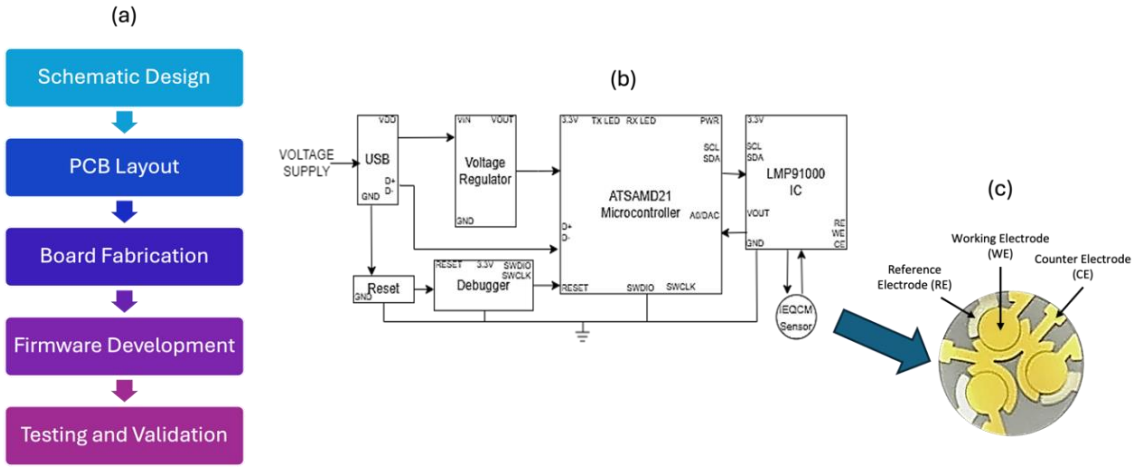

Figure 1.(a) Design Flowchart for the potentiostat system on flexible PCB. (b) Block diagram of the designed potentiostat system using ATSAMD21 microcontroller, LMP91000 Electrochemical Integrated Circuit (IC) and Integrated Electrochemical Quartz Crystal Microbalance (IEQCM) Sensor. (c) IEQCM Sensor with three electrodes: Working (WE), Reference (RE) and Counter (CE).

2.1. Electrochemical Sensor

In this work, to verify the functionality of the potentiostat circuit, the readout circuit is connected to our Integrated Electrochemical Quartz Crystal Microbalance (IEQCM) which was previously described in [27]. The IEQCM combines an electrochemical and mass sensor on a single device [27]. A single IEQCM device has three identical quartz crystal microbalance and electrochemical biosensors were placed on a single piezoelectric substrate as seen in Fig. 1(c) [28]. This sensor has the advantage of having dual functionalities in a single measurement platform. For this manuscript, we will focus on the sensor's functionality as a three-electrode electrochemical sensor that can monitor signal responses during oxidation-reduction (redox) reactions.

For this electrochemical sensor, the chemical reactions take place at the surface of the working electrode (WE) and counter electrode (CE). The potential difference between WE and CE was measured with respect to the reference electrode (RE). The measured potential difference results from the movement of ions between the three electrodes within the electrolyte solution. At the interfaces of the WE and CE, positive and negative ions combine to form an electric double layer (EDL). Consequently, alterations in the kinetics of electron transfer during redox processes within this EDL region led to changes in impedance and current which can be analysed using cyclic voltammetry.

2.2. Readout Circuit

As shown in Fig. 1(b), the sensor readout circuit comprises the LMP91000, ATSAMD microcontroller, USB port, debugger, voltage regulator, reset button, resistors and capacitors. The LMP91000 potentiostat is used to convert electrochemical reactions into measurable signals. This potentiostat IC has been used for accurate and sensitive detection of analytes [29]. ATSAMD21, a 32-bit microcontroller with on-board debugger (nEDBG) was used as the brain of the potentiostat. The ATSAMD21 has six serial communication modules (SERCOM) which are configurable as UART/USART, SPI or I^2C. In addition, it has three 16-bit timer/counters, a 32-bit real-time clock and calendar, 20 PWM channels, one 14-channel, 12-bit ADC and one 10-bit DAC. The ATSAMD21 microcontroller was chosen as it has low-power attributes which help to ensure efficient energy usage, while maintaining its high-performance capabilities that allow rapid and precise signal processing.

An important component in the potentiostat circuit is the voltage regulator which regulates the voltage supplied to various sections of the circuit, ensuring consistent and reliable operation across changing input conditions. Next is the USB port which facilitates data transfer and power input. A J-link debugger connector was also added to assist in debugging and programming. A jumper wire connector establishes a connection with the IEQCM sensor. Lastly, the reset button offers a user-friendly way to reboot the system, aiding in the troubleshooting and initialization process. Other essential elements like 10kΩ and 330Ω resistors, 0.1µF, 2.2µF and 12pF capacitors, 220Ω ferrite bead, 32.768kHz crystal and LEDs, were also added to the potentiostat circuit. Passive components are integral for stabilising voltage levels, filtering noise, and ensuring that the circuit functions properly. LEDs were also added to provide visual indications of the device's status and operations and to facilitate troubleshooting. All these components were chosen for their compatibility with the flexible substrate of the board.

The potentiostat circuit's board was designed using Altium PCB Designer, an electronics design software that comprises schematic design, circuit routing layout for the PCB, and generating the standard outputs files for board fabrication. After the circuit design was completed, the Gerber RS-274X file was generated and then shared with the PCB manufacturer, Jabil Circuit Sdn. Bhd for fabrication. The potentiostat circuit layout design is shown in Fig. 2(a).

3. EXPERIMENTAL WORK

The experimental work involved fabricating and testing multiple versions of the potentiostat design to optimise its performance and characteristics. The firmware development was programmed using Arduino after board fabrication. Subsequently, testing and validation were conducted once the fabricated board was programmed, assessing its functionality using a baseline solution.

3.1. PCB Fabrication and Assembly

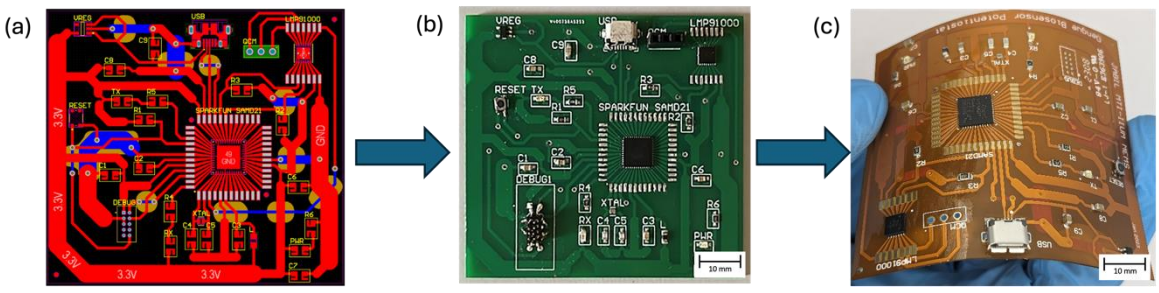

Figure 2(a) Printed Circuit Board layout design of the potentiostat system in Altium Designer. Fabricated potentiostat on a rigid PCB (b) and flexible PCB (c).

There were three versions of circuit board design implementations. The first board was fabricated on FPCB made from polyimide (PI) film with dimensions of 80.0mm x 92.0mm. This board had problems supplying accurate voltages to the sensor. This FPCB was difficult to debug as the design was compact, and its components were difficult to detach and resolder. To rectify this, a second design was fabricated on a 63.0mm x 68.0mm rigid PCB. This rigid design is shown in Fig. 2(b) and its functionality was verified. This design, while functioning, was difficult to debug, and required wire and header replacements. The final version of the potentiostat circuit was printed on a flexible printed circuit board (FPCB) to fit the requirements of a flexible potentiostat with the dimensions of 60.0mm x 65.0mm is shown in Fig. 2(c). Once the bare FPCBs were fabricated by the PCB manufacturer, an assembly process was performed at MTI Lab, Jabil Circuit Sdn. Bhd., Penang.

Before assembling the components on the PCB, solder was first printed on the PCB. To perform this, 96.5Sn/3.0Ag/0.5Cu (SAC305) solder paste with 88.25% metal content was mixed and deformed at 400rpm and 300rpm respectively for 60 seconds using a centrifugal mixer (Thinky Mixer Model ARE-310). This is to ensure that the solder paste was well mixed, has a uniform viscosity, and to release the air bubbles which may cause solder defects [30]. A 4 mils stencil was used to screen print solder paste using an automatic DEK Screen Printer. After that, the printed solder paste was inspected using Solder Paste Inspection (SPI) Kohyoung Aspire 2 Machine to ensure the right volume of solder paste has been applied [31]. Once the solder paste inspection was complete, ICs and components were placed on the FPCB using the Fuji NXT3 Pick and Place machine. Then, the populated FPCB was moved to the 10 zones reflow oven Vitronics XPM2 where all the electrical solder joints are formed between the FPCB and the components. The process then was continued with visual inspection to ensure there is not any defect post reflow process such as, solder bridging, billboard, cold solder and missing component. The PCB and FPCB were also checked for any shorts or open circuits.

The main advantage of FPCBs is their potential application in wearable devices that can adapt to the contours of human skin. No specific flexibility tests were conducted in this research due to the inherent flexibility of the FPCB that is already well-established and recognized in the industry. The primary focus of our study was on other performance metrics, given that the flexibility of FPCBs is a fundamental and widely acknowledged characteristic. Transformation of the rigid PCB to FPCB resulted in reduction of the board size from 63.0mm x 68.0mm rigid PCB to 60.0mm x 65.0mm for FPCB. In addition to the reduction in size, FPCBs possess the unique capability to bend, fold, and even twist without compromising functionality. This substantial reduction in size aligns with the objective of designing a compact and portable solution. The flexibility of FPCB allows for intricate circuitry within a confined footprint, while its lightweight nature ensures seamless integration into wearable devices.

3.2. Board Programming

Once the fabrication of the PCB and FPCB has been completed, the firmware is developed. To program and configure the registers of the ATSAMD21 and LMP91000, the System Management Bus (SMBus™) based on the Inter-Integrated Circuit (I²C) bus protocol was used. Both I²C bus and SMBus™ are compatible 2-wire buses, allowing easy interchangeability between master (ATSAMD21) and slave (LMP91000) with addressable slaves in this potentiostat system. The ATSAMD21 controls the registers through the Arduino Integrated Development Environment (IDE) software, enabling functions such as gain control, input waveform generation, and mode selection for electrochemical experiments.

The electrochemical measurement firmware of the potentiostat system was coded in Arduino software. The LMP91000 chip has limitations and can only support Cyclic Voltammetry (CV), one of the most important types of electrochemical measurements. CV is an electrochemical technique used for measuring the current response of a redox active solution. It is performed by changing the voltage of a working electrode and then measuring the current. From CV plot, electrochemical reversibility, electrokinetic behaviour and electrochemical stability of the electron transfer on the electrode-electrolyte interface can be studied. Only CV measurement instructions were coded and used in this IEQCM biosensor potentiostat system.

The firmware of the potentiostat system relies heavily on intricate code segments, each playing a pivotal role in ensuring the system's functionality and efficiency. One of the most important code segments which serves as the backbone for Cyclic Voltammetry (CV) measurements is on how to sweep the voltage from positive to negative values by varying the voltage bias. The code segment is shown in Fig. 3(a) below:

(a)

```
pstat.setNegBias();
  for (int i = 1; i <= incrV+1; i++)
  {
   pstat.setBias(i);
   delay(settling_time);
   uint16_t adcVal = analogRead(A0);
   Serial.print(millis());
   Serial.print("\t");
   Serial.print(-1*TIA_BIAS[i]*lmp_vcc);
   Serial.print("\t");
   Serial.print(adcVal);
   Serial.print("\t");
   Serial.print(pstat.getCurrent(adcVal, aref_voltage, adc_bits)*1000000,4);
   Serial.println();
  }
  for (int i = incrV; i >= 0; i--)
  {
   pstat.setBias(i);
   delay(settling_time);
   uint16_t adcVal = analogRead(A0);
   Serial.print(millis());
   Serial.print("\t");
   Serial.print(-1*TIA_BIAS[i]*lmp_vcc);
   Serial.print("\t");
   Serial.print(adcVal);
   Serial.print("\t");
   Serial.print(pstat.getCurrent(adcVal, aref_voltage, adc_bits)*1000000,4);
   Serial.println();
  }
```

(b)

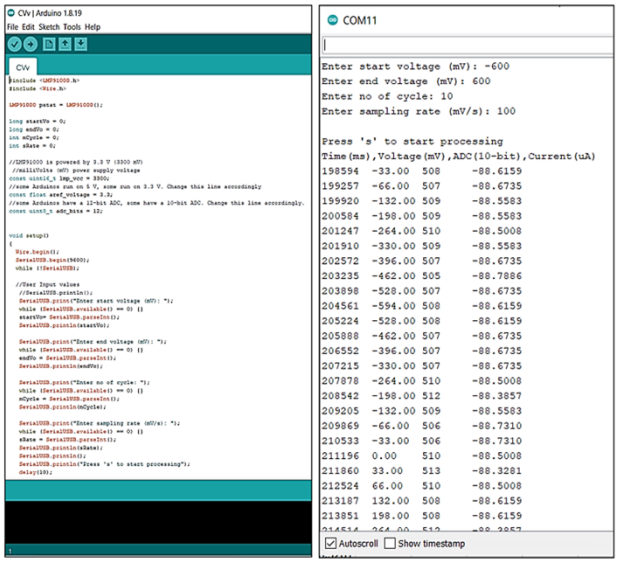

Figure 3(a) Code segment for Cyclic Voltammetry implementation on Arduino. (b) CV program and output of the potentiostat system in Arduino's serial monitor.

3.3. Electrochemical Measurement

To verify the functionality of the potentiostat circuit on PCB and FPCB, the CV technique was used to measure the sensor's current response when redox reactions occur on the sensing surface. The experimental setup is shown in Fig. 4(a) and comprises of the IEQCM sensor housed in a 3D-printed fluidic chamber connected to the designed potentiostat. The IEQCM sensor was sandwiched between silicone layers to avoid leakage. Approximately 0.1mL of the 0.5mM potassium ferrocyanide solution was drop casted on the IEQCM housed in a fluidic chamber using a 1.0mL syringe. The IEQCM sensor was connected to the potentiostat board via wires.

The flowchart for CV measurement is illustrated in Fig. 4(b). The CV program starts with supplying DC voltage to the system, changing the voltage of the working electrode of the IEQCM sensor and measuring the resulting current. The resulting output current obtained from Arduino's serial monitor was exported to Excel for further analysis (Fig. 3(b)). The CV graph allowed visualisation of the electrochemical behaviour, and various parameters, such as peak potential, peak current, and redox potential, could be extracted from the plot to verify the functionality and performance of IEQCM sensor integrated with the potentiostat.

(a)

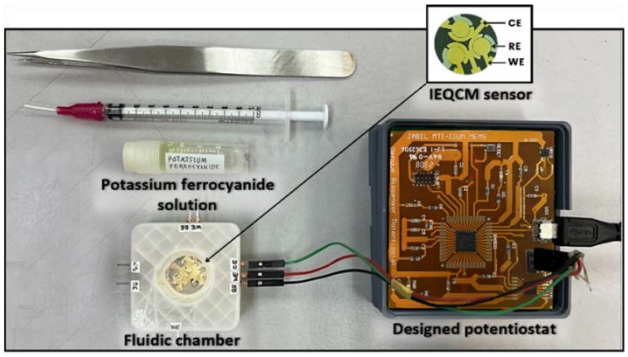

(b)

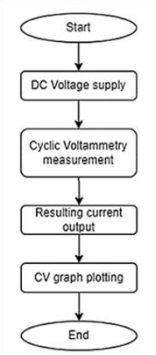

Figure 4(a) Experimental setup for the Cyclic Voltammetry measurements using the Flexible Printed Circuit Board (FPCB) potentiostat system. (b) CV measurement flowchart.

The CV measurements were performed using both the rigid and FPCB designs of the potentiostat board. Specific parameters were applied for the CV measurement, including a voltage sweep encompassing the range of -600mV to 600mV over 15 cycles, all performed at a scan rate of 100mV/s. A 0.5mM solution of potassium ferrocyanide was employed as a redox couple to explore the kinetics of heterogeneous electron transfer reactions occurring within the sensor. The electrochemical measurements obtained using the PCB and

FPCB were also compared with measurements made using a commercial portable potentiostat, Emstat to validate the outcomes of the designed potentiostats.

4. RESULTS AND DISCUSSION

The CV measurements were performed by connecting the IEQCM to the designed potentiostat. To ensure that a good CV plot is obtained, the internal resistance of the potentiostat is tuned by using several load resistances. Once the optimum R_{load} was obtained, CV measurements of both the PCB and FPCB designs were compared with measurements made using a commercial potentiostat, Emstat Pico Development Kit. Based on these results the separation between voltage peaks, ΔE_p and standard rate constants, K_s for both designs were evaluated.

4.1. Electrochemical Reversibility

The CV's current responses produced by redox reactions at the surface of the IEQCM sensor can be used to analyse the electrochemical reversibility of the IEQCM sensor. The concept of electrochemical reversibility pertains to the speed at which electrons are transferred at the interface between an electrode and a solution in a redox reaction. This process is fundamental to the behaviour of redox couples. Determining electrochemical reversibility involves analysing the separation between the anodic peak potential (E_{pa}) and the cathodic peak potential (E_{pc}) in CV measurement, which is referred to as the peak-to-peak potential (ΔE_p) [26]. Mathematically, ΔE_p is calculated as $\Delta E_p = E_{pa} - E_{pc}$. This parameter serves as an indicator of the degree of reversibility of the redox reaction. The values of ΔE_p have specific interpretations:

- Reversible: $\Delta E_p \approx 0.06V$.
- Quasi-reversible: $\Delta E_p > 0.06V$ (with presence of both peaks).
- Irreversible: $\Delta E_p < 0.06V$ (with absence of peak for reverse scan).

The CV plots obtained using the experimental setup shown in Fig. 4 were used to tune the LMP91000's internal resistance, denoted by R_{gain} (kΩ) and R_{load} (Ω). Various combinations of the R_{gain} (kΩ) and R_{load} (Ω) values were explored to optimise the CV measurement as detailed in Table 2. The internal resistance values can be adjusted according to the desired value that gives the smallest ΔE_p in the CV plot. ΔE_p is the separation between the oxidation and reduction peaks. The configuration with R_{load} = 50Ω and R_{gain} = 35kΩ emerged as the most effective, yielding superior results with the smallest ΔE_p value which contributes to increased sensitivity, enabling the detection of low analyte concentrations and subtle electrochemical changes as seen in Fig. 5. This configuration was employed for subsequent CV measurements, run at a 100mV/s scan rate, sweeping the voltage from -400mV to 600mV for 15 cycles.

Table 2. Variation of Internal Resistance Values for the Potentiostat using LMP91000

Internal Resistance	Values
R_{gain} (kΩ)	2.75, 3.5, 7, 14, 35, 120, 350
R_{load} (Ω)	10, 33, 50, 100

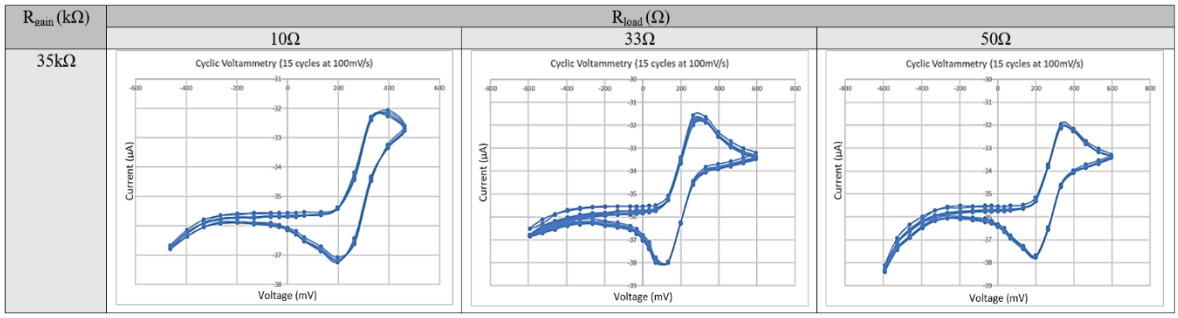

Figure 5. CV measurement results using fixed R_{gain} = 35kΩ and varying R_{load} = 10 Ω, 33Ω and 50Ω. The optimum R_{load} = 50Ω, produced distinct redox and oxidation peaks.

To assess the performance of the designed potentiostat, CV measurements were also conducted using a commercial potentiostat, the EmStat Pico development kit as shown in Fig. 6(a). The CV pattern produced by the designed potentiostat (Fig. 6(b)) is similar to the CV pattern of the EmStat Pico development kit (Fig.6(a)). EmStat Pico produced ΔE_p of 0.133V, while both the rigid PCB and FPCB produced ΔE_p of 0.132V. Both ΔE_p values show a quasi-reversible electrochemical behaviour of the system, signifying visible peak features that indicate a certain level of reversibility in the redox reactions at the electrode-solution interface of the IEQCM sensor. This consistency is significant since both designs share the same PCB design but have

different substrates. The ΔE_p values, exceeding 0.06V and the presence of both peaks, indicate that the reaction on the IEQCM sensor is quasi-reversible. This observed behaviour further signifies that the redox process is diffusion-controlled in nature, aligning with the underlying principles of the system [22].

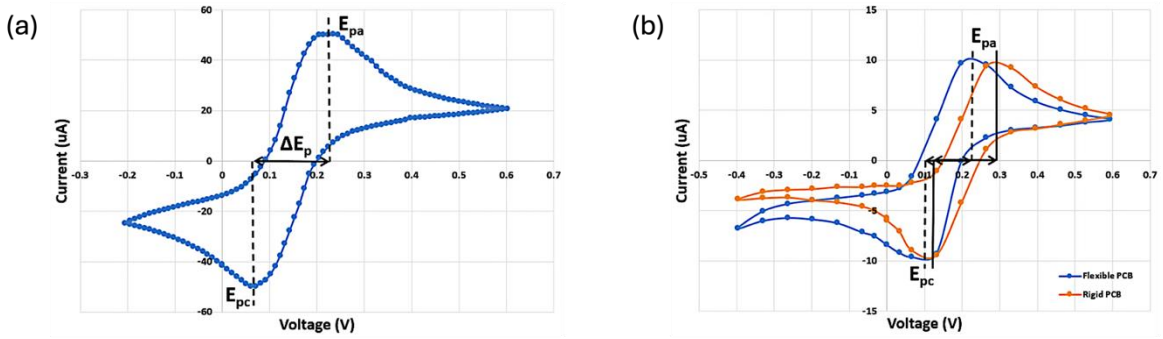

Figure 6(a). Cyclic Voltammetry (CV) measurement of Voltage (mV) against Current (μA) at 100mV/s scan rate using EmStat Pico development board. (b) CV measurement of Voltage (mV) against Current (μA) at 100mV/s scan rate using both rigid PCB and FPCB potentiostat.

In terms of peak current, the rigid PCB has ΔI_p value of 18.65μA, while the FPCB has ΔI_p of 19.31μA. This substantial increase in peak current suggests that there is efficient transfer of electrons from the solution to the electrode which can be detected by both PCB designs. The higher ΔI_p value in the FPCB emphasises its superior electron transfer capability, attributed to the integrated IEQCM design and excellent electrical conductivity [24]. Though the peak current height observed with the commercial potentiostat is higher than that measured with our designed potentiostat, this discrepancy can be attributed to the high-specification components and optimised design architectures of commercial potentiostats which allow them to achieve superior performance in terms of sensitivity and signal amplification. In contrast, our designed potentiostat prioritises cost-efficiency and flexibility, especially for wearable applications. Consequently, it utilises more affordable components and simpler design approaches. However, it is important to note that our primary focus is not on the peak current height but rather on the peak potential (ΔE_p). The peak potential is a critical parameter for our applications, and our designed potentiostat demonstrates minimal variation in ΔE_p compared to the commercial potentiostat. This indicates that, despite the differences in peak current detection, our device provides accurate and reliable peak potential measurements which are essential for its intended applications.

4.2. Standard Rate Constant (Ks)

CV measurements can also be used to derive the standard rate constant (K_s) values. K_s of electron transfer is a measure of how quickly an electrochemical reaction takes place at an electrode surface under standard conditions [32]. In CV, K_s represents the speed at which electrons are transferred between the electrode and the electroactive species in the solution during redox reaction. It is a fundamental parameter that provides insights into the kinetics of the redox process. Nicholson's treatment is a method used to evaluate K_s, experiments combined with the Klingler and Kochi method, specifically suited for entirely irreversible systems [33]. Consequently, a system that initially appears reversible at a certain frequency can reveal kinetic behaviour at higher frequencies, as evidenced by increased differentiation between cathodic and anodic peak potentials. The K_s for electron transfer is extracted from this peak potential separation and the frequency where Ψ is kinetic parameter, F is Faraday's constant, E is the applied potential, R is the gas constant, n is the number of electrons, T is the temperature in Kelvin as shown in equation below.

$$\Psi = (-0.6288 + 0.0021\,\Delta E_p)/(1 - 0.017\,\Delta E_p) \quad (1)$$

$$\Psi = K_s\,(\pi DnVF / RT)^{-1/2} \quad (2)$$

The approach offers a rapid and straightforward means to assess electrode kinetics. The consistent K_s value of 0.0036cm/s obtained for both PCB types as seen in Fig. 7 shows the reliability and reproducibility of our experimental setup and measurement techniques. This value is indicative of the intrinsic electron transfer kinetics of the system and reflects the consistency of our methodology, while acknowledging the potential subtle differences due to substrate variations. These findings show the ability to provide reliable electrochemical data under varying PCB substrate materials.

Table 4 compares the peak currents and peak voltage of CV measured with different potentiostats. It can be seen that while the peak current is lower in the designed potentiostat, the peak voltage is still comparable to the Emstat, Ministat and KickStat. The main limitation in functionality of this designed board is due to the limitation of the LMP91000, which can only handle CV measurements. This is an expected tradeoff due to the low cost of the LMP91000 chip (USD 3.30) compared to EmStat Pico (USD 500). For wearable applications, such as glucose detection in sweat, lower cost is preferred compared to extensive functionalities at the expense of higher cost.

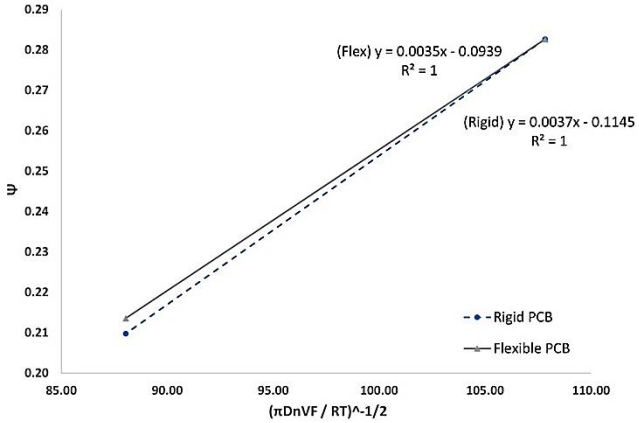

Figure 7. Standard Rate Constant (K_s) of both rigid and flexible Printed Circuit Board (PCB) potentiostat.

Table 4. Internal Resistance Values of LMP91000 Electrochemical Sensor

Potentiostat	PCB Type	Peak Current (μA)	Peak Voltage (mV)	Limitations	Ref
MiniStat	Rigid	13.3	270	Dependency on the laboratory potentiostat. Limited software.	[19]
KickStat	Rigid	14.39	200	Lower peak current.	[6]
EmStat Pico	Rigid	163.0	340	Requires proficiency in a specific scripting language, MethodSCRIPT. High cost compared to other portable potentiostat.	[23]
EmStat Pico (This work)	Rigid	84.0	255	Requires proficiency in a specific scripting language, MethodSCRIPT. High cost compared to other portable potentiostat.	-
Designed Potentiostat (This work)	Flexible	10.3	264	Limited electrochemical measurement functionality (Only CV)	-

5. CONCLUSION

In this work, the development of a portable data acquisition system for electrochemical measurements, using both FPCB and PCB designs were reported. The dimensions of the compact and portable design on FPCB are 60.0mm x 65.0mm. The FPCB potentiostat was functional and validated for CV measurements using ferrocyanide and produced a ΔE_p value of 0.132V compared to 0.133V of the commercial EmStat Pico potentiostat. Smaller value of ΔE_p indicates sufficient sensitivities and capabilities of low analyte concentration detection. This combination of small size and satisfactory performance shows that the proposed potentiostat design on FPCB has great potential for various electrochemical studies in wearable applications. In conclusion, this research shows the proof of concept that a low cost, functional potentiostat can be implemented on a flexible polyimide printed circuit board.

ACKNOWLEDGEMENTS

This project is a collaborative work between VLSI-MEMS Research Unit and by Manufacturing Technology and Innovation (MTI) Lab, Jabil Circuit Sdn. Bhd. Penang. The flexible potentiostat boards in this work were fabricated by Manufacturing Technology and Innovation (MTI) Lab, Jabil Circuit Sdn. Bhd.

Penang. The authors also wish to thank the Malaysian Ministry of Higher Education for funding this project under the PRGS grant: PRGS/2/2019/SKK14/USM/02/1.

REFERENCES

[1] P. Escobedo, L. Manjakkal, M. Ntagios, and R. Dahiya, "Flexible Potentiostat Readout Circuit Patch for Electrochemical and Biosensor Applications," *FLEPS 2020 - IEEE International Conference on Flexible and Printable Sensors and Systems*, pp. 20–23, 2020, doi: 10.1109/FLEPS49123.2020.9239515.

[2] K. Nam, G. Choi, H. Kim, M. Yoo, and H. Ko, "A Potentiostat Readout Circuit with a Low-Noise and Mismatch-Tolerant Current Mirror Using Chopper Stabilization and Dynamic Element Matching for Electrochemical Sensors," *Applied Sciences 2021, Vol. 11, Page 8287*, vol. 11, no. 18, p. 8287, Sep. 2021, doi: 10.3390/APP11188287.

[3] I. Jeerapan and S. Khumngern, "Printed Devices for Wearable Biosensors: Laboratory to Emerging Markets," *IEEE Journal on Flexible Electronics*, vol. 2, no. 5, pp. 1–1, 2023, doi: 10.1109/jflex.2023.3272624.

[4] H. Zhao *et al.*, "Recent advances in flexible and wearable sensors for monitoring chemical molecules," *Nanoscale*, vol. 14, no. 5, pp. 1653–1669, Feb. 2022, doi: 10.1039/D1NR06244A.

[5] A. Vanhooydonck, T. Caers, M. Parrilla, P. Delputte, and R. Watts, "Achieving High-Precision, Low-Cost Microfluidic Chip Fabrication with Flexible PCB Technology," *Micromachines (Basel)*, vol. 15, no. 4, p. 425, Apr. 2024, doi: 10.3390/MI15040425/S1.

[6] O. S. Hoilett, J. F. Walker, B. M. Balash, N. J. Jaras, S. Boppana, and J. C. Linnes, "Kickstat: A coin-sized potentiostat for high-resolution electrochemical analysis," *Sensors (Switzerland)*, vol. 20, no. 8, Apr. 2020, doi: 10.3390/s20082407.

[7] I. C. Ezema Ike-Eze *et al.*, "An Overview of Flame Retardants in Printed Circuit Boards for LEDs and other Electronic Devices," *J. Mater. Environ. Sci*, vol. 2023, no. 4, pp. 410–420, 2023, [Online]. Available: http://www.jmaterenvironsci.com

[8] Y. Wang *et al.*, "Review—Flexible and Stretchable Electrochemical Sensing Systems: Materials, Energy Sources, and Integrations," *J Electrochem Soc*, vol. 167, no. 3, p. 037573, Mar. 2020, doi: 10.1149/1945-7111/AB7117.

[9] R. Shi, S. Wang, Z. Xia, L. Lu, and M. Wong, "Fluorinated Metal-Oxide Thin-Film Transistors for Circuit Implementation on a Flexible Substrate," *IEEE Journal on Flexible Electronics*, vol. 1, no. 1, pp. 58–63, Dec. 2021, doi: 10.1109/JFLEX.2021.3140044.

[10] C. Choi, H. Seung, and D.-H. Kim, "Bio-Inspired Electronic Eyes and Synaptic Photodetectors for Mobile Artificial Vision," *IEEE Journal on Flexible Electronics*, vol. 1, no. 2, pp. 76–87, Mar. 2022, doi: 10.1109/JFLEX.2022.3162169.

[11] J. Song and F. Yan, "Applications of Organic Electrochemical Transistors in Flexible Bioelectronics," *IEEE Journal on Flexible Electronics*, vol. 1, no. 2, pp. 88–97, Jun. 2022, doi: 10.1109/JFLEX.2022.3179674.

[12] T. E. Paterson *et al.*, "Monitoring of hand function enabled by low complexity sensors printed on textile," *Flexible and Printed Electronics*, vol. 7, no. 3, p. 035003, Jul. 2022, doi: 10.1088/2058-8585/AC7DD1.

[13] R. R. Nair, "Glucose sensing and hybrid instrumentation based on printed organic electrochemical transistors," *Flexible and Printed Electronics*, vol. 5, no. 1, p. 015001, Jan. 2020, doi: 10.1088/2058-8585/AB63A0.

[14] L. Mo *et al.*, "Full printed flexible pressure sensor based on microcapsule controllable structure and composite dielectrics," *Flexible and Printed Electronics*, vol. 6, no. 1, p. 014001, Mar. 2021, doi: 10.1088/2058-8585/ABE842.

[15] W. Zhao, S. Tian, L. Huang, K. Liu, and L. Dong, "The review of Lab-on-PCB for biomedical application," *Electrophoresis*, vol. 41, no. 16–17, pp. 1433–1445, Sep. 2020, doi: 10.1002/ELPS.201900444.

[16] J. Yao *et al.*, "A Portable Potentiostat for Three-Electrode Electrochemical Sensor," *Journal of Physics: Conference Series PAPER • OPEN ACCESS Journal of Physics: Conference Series*, vol. 1550, p. 42049, 2020, doi: 10.1088/1742-6596/1550/4/042049.

[17] O. Alao, "(PDF) Online condition monitoring of Lithium-ion and Lead acid batteries for renewable energy applications." Accessed: Jan. 17, 2023. [Online]. Available: https://www.researchgate.net/publication/333403369_Online_condition_monitoring_of_Lithium-ion_and_Lead_acid_batteries_for_renewable_energy_applications

[18] J. Cook, "SIMstat: Hardware Design Considerations for Implementing a Low-Cost, Portable Potentiostat," 2020.

[19] S. D. Adams, E. H. Doeven, K. Quayle, and A. Z. Kouzani, "MiniStat: Development and Evaluation of a Mini-Potentiostat for Electrochemical Measurements," *IEEE Access*, vol. 7, pp. 31903–31912, 2019, doi: 10.1109/ACCESS.2019.2902575.

[20] D. M. Jenkins, B. E. Lee, S. Jun, J. Reyes-De-Corcuera, and E. S. McLamore, "ABE-Stat, a Fully Open-Source and Versatile Wireless Potentiostat Project Including Electrochemical Impedance Spectroscopy," *J Electrochem Soc*, vol. 166, no. 9, pp. B3056–B3065, 2019, doi: 10.1149/2.0061909jes.

[21] L. E. Sebar, L. Iannucci, E. Angelini, S. Grassini, and M. Parvis, "Electrochemical Impedance Spectroscopy System Based on a Teensy Board," *IEEE Trans Instrum Meas*, vol. 70, 2021, doi: 10.1109/TIM.2020.3038005.

[22] S. A. Perdomo *et al.*, "SenSARS : A Low-Cost Portable Electrochemical Diagnostics of SARS-CoV-2 Infections," *IEEE Trans Instrum Meas*, vol. 70, pp. 1–10, 2021.

[23] L. Stratmann, "EMStat Pico: An Electrochemical System On Module for Integration of Standard Analysis Methods with a Minimum of Development Effort," 2019.

[24] H. Shamkhalichenar, C. J. Bueche, and J. W. Choi, "Printed Circuit Board (PCB) Technology for Electrochemical Sensors and Sensing Platforms," *Biosensors*, vol. 10, no. 11. NLM (Medline), Oct. 30, 2020. doi: 10.3390/bios10110159.

[25] A. A. Zainuddin, "Integrated electrochemical and mass biosensor for early dengue detection," 2020, Accessed: Nov. 18, 2022. [Online]. Available: http://studentrepo.iium.edu.my/handle/123456789/10088

[26] A. Benoudjit, "A STABLE SOLID CONTACT TRANSDUCER AND IONOPHORE-FREE ALL-SOLID-STATE AMMONIUM ION-SELECTIVE ELECTRODE FOR MOBILE SENSOR APPLICATION IN AQUEOUS MEDIA," 2021.

[27] D. Plausinaitis, L. Sinkevicius, U. Samukaite-Bubniene, V. Ratautaite, and A. Ramanavicius, "Evaluation of electrochemical quartz crystal microbalance based sensor modified by uric acid-imprinted polypyrrole," *Talanta*, vol. 220, p. 121414, Dec. 2020, doi: 10.1016/J.TALANTA.2020.121414.

[28] A. A. Zainuddin *et al.*, "Development of integrated electrochemical-quartz crystal microbalance biosensor arrays: Towards ultrasensitive, multiplexed and rapid point-of-care dengue detection," in *BIODEVICES 2019 - 12th International Conference on Biomedical Electronics and Devices, Proceedings; Part of 12th International Joint Conference on Biomedical Engineering Systems and Technologies, BIOSTEC 2019*, SciTePress, 2019, pp. 220–227. doi: 10.5220/0007523802200227.

[29] Texas Instruments, "LMP91000 Sensor AFE System: Configurable AFE Potentiostat for Low-Power Chemical-Sensing Applications," 2014. [Online]. Available: www.ti.com

[30] E. Wernicki *et al.*, "Preparation and characterization of nano-solder paste with high nanoparticle loading and their thermal and printing properties," *Mater Chem Phys*, vol. 297, p. 127399, Mar. 2023, doi: 10.1016/J.MATCHEMPHYS.2023.127399.

[31] E. Griffith and S. P. Lim, "Evolution and Applications of Fine-Feature Solder Paste Printing for Heterogeneous Integration," *International Symposium on Microelectronics*, vol. 2021, no. 1, pp. 000362–000367, Oct. 2021, doi: 10.4071/1085-8024-2021.1.000362.

[32] "Figure 1. Cyclic polarograms showing effect of charge transfer coefficient, a".

[33] I. Lavagnini, R. Antiochia, and F. Magno, "An Extended Method for the Practical Evaluation of the Standard Rate Constant from Cyclic Voltammetric Data", doi: 10.1002/elan.200302851.